Articles

Model for a Helical Bundle Channel Based on the High-Resolution Crystal Structure of Trichotoxin_A50E†

J. K. Chugh,‡ H. Brückner,§ and B. A. Wallace*,‡

Department of Crystallography, Birkbeck College, University of London, London WC1E 7HX, U.K., and Department of Food Sciences, Interdisciplinary Research Center, University of Giessen, Giessen, Germany

Received May 17, 2002; Revised Manuscript Received August 7, 2002

ABSTRACT: Trichotoxin_A50E is an 18-residue peptaibol antibiotic which forms multimeric transmembrane channels through self-association. The crystal structure of trichotoxin has been determined at a resolution of 0.9 Å. The trichotoxin sequence contains nine helix-promoting Aib residues, which contribute to the formation of an entirely helical structure that has a central bend of 8−10° located between residues 10−13. Trichotoxin is the first solved structure of the peptaibol family that is all α-helix as opposed to containing part or all 3_{10}-helix. Gln residues in positions 6 and 17 produce a polar face, and are proposed to form the channel lumen. An octameric model channel has been constructed from the crystal structure. It has a central pore of ∼4−5 Å radius, a size sufficient to enable transport of ions, with a constricted region at one end, formed by a ring of Gln6 residues. Electrostatic calculations are consistent with it being a cationic channel.

The peptaibols are a family of antibiotic polypeptides that exhibit antibacterial activity mainly against gram-positive bacteria. These peptides are produced by soil fungi and range in length from five to twenty residues. Longer members of the family are capable of inserting into lipid bilayer membranes, forming multimeric ion channels.

Most peptaibols have an acetylated N-terminus, a C-terminal amino alcohol, and a frequent occurrence of the nonstandard, helix-promoting amino acid Aib (α-aminoisobutyric acid or α-methylalanine). The sequences of over 250 peptaibols have been compiled in the peptaibol database located at http://www.cryst.bbk.ac.uk/peptaibol.

The peptaibols have been divided into subfamilies (SFs)[1] on the bases of their sequences, lengths, and functional properties (*1*). The largest SF is SF1, containing the "long" peptaibols, which are between seventeen and twenty residues in length. The trichotoxins are members of SF1 and have been isolated from the fungus *Trichoderma viride* strain NRRL 5242 (*2*−*6*). So far, structures of two other SF1 members have been described: the crystal structure of alamethicin_F30 (*7*) and the NMR solution structure of chrysospermin_C (*8*). These peptaibols have functionally significant differences in sequence from the trichotoxins (Figure 1).

```
Trichotoxin_A50E    Ac-UGULU-QUUUAAUPLUU-QV-ol
Trichotoxin_A40_1   Ac-UGULU-QUUAAUUPLUU-EV-ol
Alamethicin_F30     Ac-UPUAUAQUVUGLUPVUUEQF-ol
Chrysospermin_C     Ac-FUSUJLQGUUAAUPUUU-QW-ol
```

FIGURE 1: The sequences of trichotoxin_A50E, trichotoxin_A40-1, alamethicin_F30, and chrysospermin_C. Imino acid residues are in yellow, aromatics in red. Glu is in green and Gln in blue. U = Aib, and J = Iva. Alignments were done in CINEMA (*9*).

MATERIALS AND METHODS

Synthesis and Crystallization. The trichotoxin_A50E peptide was prepared by solution phase synthesis as previously described (*6*), and was characterized by mass spectrometry and liquid chromatography. Crystals were obtained from a mixture of methanol and acetonitrile at a ratio of 1:10 (v/v), using a peptide concentration of 29.6 mg/mL at 4 °C.

Data Collection. Data were collected on the Synchrotron Radiation Source at Daresbury using the high-resolution microfocus Station 9.8. A single crystal of dimensions 0.01 × 0.06 × 0.01 mm^3 was used for data collection at −123 °C. The data were collected to a resolution of 0.8 Å. Due to deterioration of data quality in the final 0.8−0.9 Å shell, as determined by I/SigI, only data to 0.9 Å was processed using the BRUKER SHELXTL package (*10*) and used for structure solution. The Rσ for the 0.9 Å data was 0.059 and Rint was

† J.K.C. was supported by a BBSRC studentship. Data collection at the Daresbury Synchrotron Radiation Source Station 9.8 was supported by a beamtime grant from the BBSRC to B.A.W.

* To whom correspondence should be addressed. E-mail: ubcg25a@mail.cryst.bbk.ac.uk. Fax: +44 (0)207-631-6803. Phone +44 (0)207-631-6857.

‡ Department of Crystallography.

§ Department of Food Sciences.

[1] Abbreviations: Ac, acetyl; MeCN, acetonitrile; MeOH, methanol; Hyp, hydroxyproline; U, α-aminoisobutyric acid; J, isovaline; CGLS, conjugated gradient least squares; NMR, nuclear magnetic resonance; RMSD, root-mean-square deviation; SF, subfamily; Vol, valinol.

10.1021/bi026150z CCC: $22.00
Published on Web 10/04/2002

Table 1: Statistics for the Trichotoxin Crystal Structure Determination and Refinement[a]

space group	*P*1
unit cell	$a = 9.455$, $b = 16.75$, $c = 31.68$ Å, $\alpha = 95.77°$, $\beta = 98.07°$, $\gamma = 99.45°$
solvent content	8.3%
mol/au	2
resolution	0.9 Å
redundancy	2.79 (2.18)
completeness	99.7% (99.9%)
Rσ	0.059 (0.413)
Rint	0.051 (0.261)
no. of total unique reflections	14115
final Rfactor	0.075
final Rfree	0.092
no. of non-H atoms	238
no. of solvent atoms (non-H)	11
average B-factors (Å^2)	
chain A	4.03
chain B	4.37
RMSD (chains A and B)	1.18 Å

[a] Values in parantheses are for the outermost resolution shell, 0.90−0.95 Å.

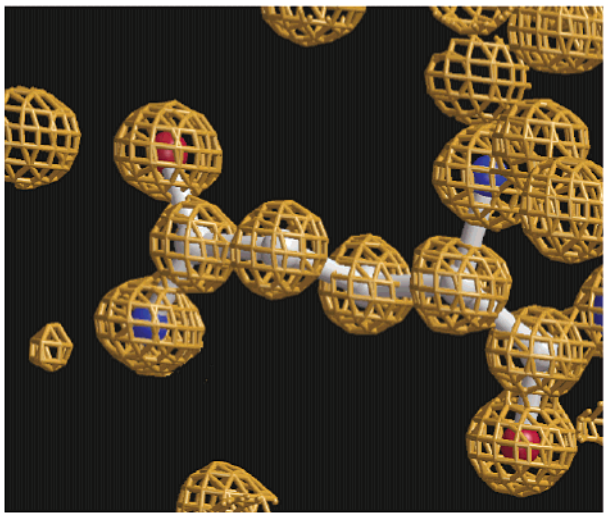

FIGURE 2: Electron density (2Fo−Fc) map, showing the atomicity at this resolution. The density around Gln17 of chain A is shown. The map is contoured at 1.6σ. This figure was made using BOBSCRIPT v.2.3 (*20*) and RASTER3D (*21*).

0.051. Data completeness was 99.7%. The outermost resolution shell from 0.95 to 0.90 Å had an Rσ of 0.413, Rint of 0.261, and redundancy of 2.18 (Table 1).

Molecular Replacement. A Matthews coefficient calculation (*11*) suggested the crystals had 8.3% solvent content, and two molecules in the asymmetric unit. Such a low solvent content is consistent with other peptaibol crystals: antiamoebin and alamethicin had solvent contents of 28 and 30%, respectively (*12*, *7*). The structure described in this paper was determined by molecular replacement, although virtually identical structures were also obtained from these data by two different direct methods procedures (Chugh and Wallace, in preparation). A wide range of truncated models derived from the alamethicin crystal structure were unsuccessful using both AmoRe (*13*) and MOLREP (*14*) procedures. The structure was ultimately solved using a theoretical helical model for the first 12 residues and the N-terminal acetyl (Ac) group, initially created in the molecular graphics program SYBYL, version 6.7 (*15*). The solution was obtained using MOLREP, and included two molecules in the asymmetric unit. The search model had 75 (non-hydrogen) atoms out of the 119 atoms expected for trichotoxin_A50E. *B*-factors were set to 20. The molecular replacement search using data between 10 and 4 Å resolution resulted in a solution with a correlation coefficient of 0.516 and an Rfactor of 0.486. The solution was initially refined in SHELXL (*16*) using data between 11 and 2.1 Å. At this stage the Rfactor was 0.457 and the Rfree was 0.531. Then 40 cycles of CGLS (conjugated gradient least squares) refinement were done using data to a resolution of 1.3 Å, producing an Rfactor of 0.425 and Rfree of 0.455.

Arp/Warp (*17*) was then used to identify additional atoms: After a total of 100 rigid body refinement cycles with model building every 10 cycles, the Rfactor decreased to 0.136 and Rfree to 0.152. At this stage the peptide structure was made up of only Ser, Ala, and Gly residues with a connectivity index of 89%. However, chain B lacked the three C-terminal residues, so the procedure was repeated to include data to 0.9 Å resolution. The C-termini residues of both chains A and B were then accounted for, but this resulted in a slightly higher Rfactor of 0.151 and Rfree of 0.167.

Model Building and Refinement. Model building of the polypeptides was carried out using the program O, version 8 (*18*) to produce the correct amino acid sequences. One acetonitrile (MeCN) molecule was also built into density. Refinement was carried out in SHELXL. Each chain was defined as a rigid body and 20 cycles of full matrix least-squares refinement were performed with data to 1.3 Å resolution. Aib, Ac, MeCN, and valinol (Vol) were defined in the .ins file by use of the HIC−UP heterocompound database (*19*), which generated appropriate parameters for the unusual residues. Then 50 cycles of CGLS refinement at 0.9 Å with the inclusion of antibumping restraints gave an Rfactor of 0.153 and Rfree of 0.164.

SHELXWAT was used to identify four water molecules. Rejection was on the basis of the isotropic U being greater than 0.2 for a potential water molecule. A further 40 cycles of CGLS refinement led to an Rfactor of 0.153 and Rfree of 0.170. Addition of two more water molecules by analysis of sigma-weighted difference maps and the introduction of anisotropy with 50 cycles of CGLS refinement gave an Rfactor of 0.108 and Rfree of 0.132.

A further MeCN molecule was added after inspection of the sigma-weighted difference maps. This, combined with rebuilding of the Leu14 side chains, addition of hydroxyl groups to the C-terminal residues and addition of hydrogens and water molecules, resulted in a final Rfactor of 0.075 and Rfree of 0.092 (Figure 2). The restrained goodness-of-fit was 0.977. The final model consists of 527 atoms including hydrogen atoms and five water and two MeCN molecules.

The coordinates and structure factors have been deposited in the Protein Data Bank as entry 1M24.

Structure Analysis Methods. PROCHECK (*22*) and WHATCHECK (*23*) were used to examine the stereochemistry, geometry, and quality of the structure. PROMOTIF (*24*) was used to define secondary structure and hydrogen bonding patterns of the peptide. MODEL from the RESTRAIN suite of programs was used for the calculation of

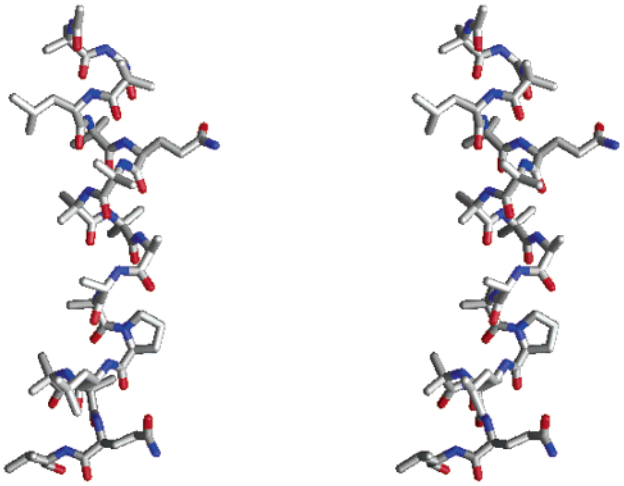

FIGURE 3: Stereoview of trichotoxin chain A. This figure was produced in GRASP (*26*).

inter- and intramolecular contacts (*25*). For RMSD, electrostatics, and dipole calculations, GRASP (*26*) was used with AMBER (*27*) charges assigned. HOLE (*28*) was used to calculate and visualize the pore diameter.

Modeling of the Channel Structure. The chain A structure was used for modeling the channel as it was better ordered than chain B. The channel model was generated using the CCP4 program PDBSET (*29*) and GRASP (*26*) with octameric symmetry. The monomers were initially oriented so that the hydrophilic Gln side chains would form a lumen and the hydrophobic Leu and Vol side chains would lie on the periphery. The octamer structure was minimized in SYBYL (*15*) with 500 cycles of CGLS refinement. The RMSD between the chain A structures before and after minimization as part of the channel with the inclusion of side chains was 0.65 Å.

RESULTS

Structural Features. Two independent peptides were found in the unit cell. These molecules were labeled chains A and B. Both chains are essentially all α-helical, including residues 2−16 in chain A and residues 2−17 in chain B (Figure 3). The termini are type I β-turns. No 3_{10}-helix was found, unlike in all other peptaibol structures solved to date. Chains A and B differ from each other slightly: chain A has a bend angle of 8° and chain B of 10°. Consequently, the length of chain A is 29.9 Å and chain B is 29.8 Å. These helices are of sufficient lengths to span the hydrophobic section of a lipid bilayer.

The trichotoxin helix is amphipathic: residues Gly2 and Gln6 contribute to the polar face, along with the carbonyl oxygen atoms of Aib9, Ala10, and Pro13. The Leu4 side chain is in different conformations in chains A and B, indicating there may be some flexibility in this residue. From residue Aib9 onward, the two monomers deviate from each other slightly. The C-terminal Vol18 residue has different conformations in the two chains. Additionally, disorder at the C-terminus of chain B was seen in the difference maps indicating two possible conformations. However, the second conformation was a minority and thus not defined enough to model a suitable conformation. The RMSD between the two trichotoxin chains is 1.18 Å for all non-hydrogen atoms, but only 0.386 Å between backbone atoms (Figure 4).

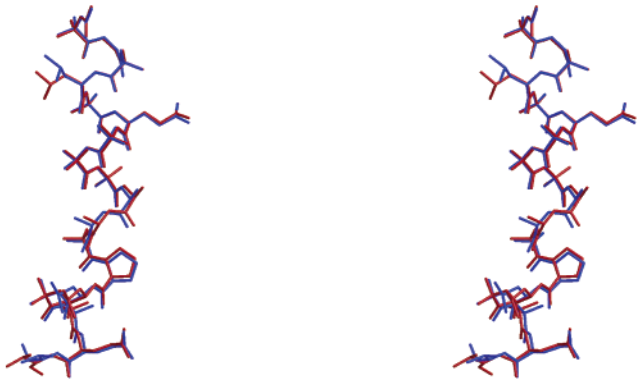

FIGURE 4: Stereoview of chains A (red) and B (blue) from the crystal structure of trichotoxin superimposed. This figure was produced in MOLSCRIPT v.2.0 (*30*) and RASTER3D (*21*).

Because the chains are so similar, unless otherwise stated, only chain A will be discussed. There are no intermolecular hydrogen bonds between the two polypeptides in the asymmetric unit. The B-factors for both chains were very low, with over 95% of the atoms having B-factors between 1 and 10.

Packing in the Crystal. The two helices in the unit cell pack in an antiparallel manner. The molecules are oriented so that their polar surfaces face inward opposite each other. The Gln17 side chains are at the N-terminal ends of the other helix allowing them to come close in a zip-like manner.

Dipoles. In this study, dipoles have been calculated using GRASP (*26*). The average dipole moment of chains A and B of trichotoxin is 37 D. By comparison, alamethicin and antiamoebin dipole moments are 54.1 and 26.8 D, respectively. These are very comparable to the experimentally measured dipole moments of alamethicin-like peptides (*31*). The differences in calculated dipoles between trichotoxin, antiamoebin, and alamethicin are accounted for by their differences in structure: Antiamoebin has three hydroxyproline and proline residues, and a greater bend (45−56°) in its structure (*12*), and aromatic residues at both the N- and C-termini, thus resulting in a weaker dipole. Alamethicin has a charged Glu residue near its C-terminus which results in its larger dipole.

Geometric Deviations from "Ideal". Residues 10−12 are not as tightly coiled as the rest of the structure. The phi−psi angles for these residues tend to be closer to those of a 3_{10}-helix, which are usually −49° and −26°, even though the hydrogen bonding pattern is that of an α-helix. The phi angle for Ala11 (−86°) is much higher than the expected −49°. This causes the carbonyl oxygen of Ala10 to protrude on the polar face of the helix. A slightly high phi angle is seen for Gln6 (−71°), resulting in its side chain protruding outward on the polar face of the helix.

It was of interest to examine the planarity of the polypeptide backbone, since the structure was solved by a full matrix least-squares procedure with no geometric constraints. In other high-resolution structures of polypeptides, the ω angle often deviates significantly from planarity (*32*, *33*), although in most large protein structures planarity is used as a geometric constraint. Both chains in trichotoxin have planar backbones within which most angles deviate by less than 10°; however, in chain A the planarity angle of Gln17 deviates by 13° and for Ala11 in chain B by 12°.

Table 2: Intramolecular Hydrogen Bonds

donor O	acceptor N	chain A length (Å)	chain A angle (deg) C=O−N	chain B length (Å)	chain B angle (deg) C=O−N
Ac	Leu4	3.02	161	2.94	162
Aib1	Aib5	2.93	154	3.00	155
Gly2	Gln6	2.97	156	2.98	157
Aib3	Aib7	2.96	157	2.99	153
Leu4	Aib8	2.99	164	3.00	158
Aib5	Aib9	2.96	148	3.00	150
Gln6	Ala10	3.01	155	3.11	155
Aib7	Ala10	3.24	110	3.19	114
Aib8	Ala11	3.06	122	2.92	125
Aib9	Aib12	3.06	117	3.06	122
Ala11	Leu14	2.94	138	2.98	135
Aib12	Aib16	3.11	163	3.09	163
Pro13	Gln17	3.44	138	3.20	141
Leu14	Gln17	3.08	118		
Leu14	Vol18			3.10	163
Aib15	Vol18	3.09	126		
Aib15	Vol18[a]			2.88	138

[a] Denotes the hydrogen bond was made to the OH group of Vol18.

PROCHECK also indicated the mean chi (χ_1) angles for Leu4 in chain A as being unusually high with a deviation of 17°. This high-resolution, geometrically unrestrained structure indicates that proteins can contain side chain conformations that are not normally produced in geometrically constrained protein structures determined at lower resolutions. Such can be observed in other high-resolution structures. The high-resolution crystal structures of ribonuclease (*32*) and crambin (*33*) both contained chi angles that were above the average of 182.7 ± 13.1°.

Hydrogen Bonding. The criteria used for hydrogen bonds were (a) a length between 2.5 and 3.5 Å and (b) an angle of ≥110° (Table 2). Chains A and B each have 15 intramolecular hydrogen bonds involving intramolecular backbone interactions. The major difference in the hydrogen bonding of the two chains is in their C-termini. In chain A, O14 makes a hydrogen bond to N17 and in chain B, O14 hydrogen bonds to N18. An influence on this is that chain A is a turn from residue 16 onward whereas in chain B this occurs from residue 17 onward. Due to the difference in conformations in the C-termini, O15 is able to hydrogen bond with OH18 (Figure 5).

There are no intermolecular hydrogen bonds between the chains. However, the two molecules do interact through a water molecule. Water molecule 4 forms hydrogen bonds to Gln6 of chain A and Gln17 chain B. Water molecules 1, 4, and 5 form hydrogen bonds to chain A and water molecules 2, 3, and 4 form hydrogen bonds to chain B. Water molecule 1 also forms two hydrogen bonds to chain A (Table 3).

Solvent Content. Five well-ordered waters and two MeCN molecules were observed. For a calculated solvent content of 8.3%, the theoretically expected number of solvent molecules was nine, so most of the solvent is ordered in these tightly packed crystals. Neither of the two MeCN molecules make any intermolecular hydrogen bonds and both have relatively high B-factors. Of the five water molecules, the two water molecules that form two hydrogen bonds each, have higher *B*-factors.

Table 3: Water Molecules Involved in Hydrogen Bonding to Polypeptide

chain	donor	acceptor water molecules (HOH)	length (Å)
A	Aib16 (O)	1	2.77
A	Vol18 (OH)	1	3.46
B	Gly2 (N)	2	2.97
B	Ala10 (O)	3	2.78
B	Gln17 (NE2)	4	2.86
A	Gln6 (NE2)	4	2.91
A	Aib12 (O)	5	2.99

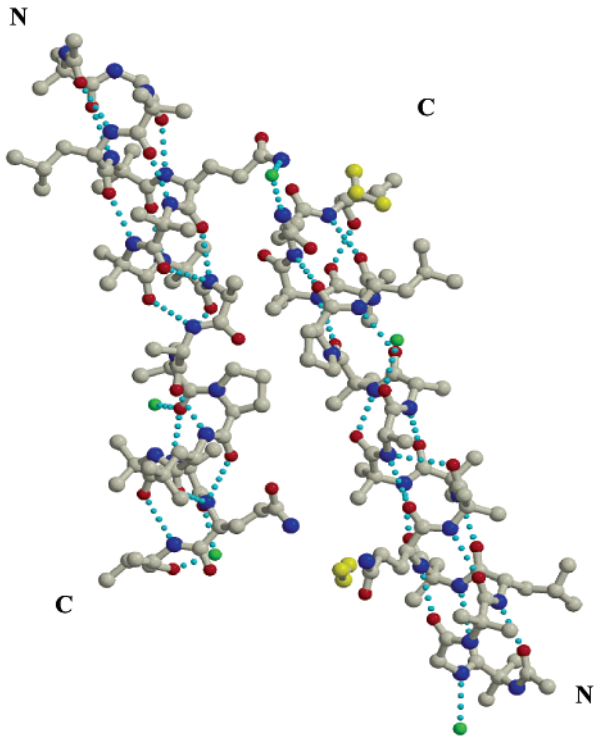

FIGURE 5: Intramolecular hydrogen bonding and hydrogen bonds between polypeptides and solvent. The two polypeptide chains in the asymmetric unit are linked by a hydrogen bond to the same water molecule. Water and acetonitrile (MeCN) molecules are shown as green and yellow spheres, respectively. Hydrogen bonds are represented by cyan-colored dotted lines. Oxygen and nitrogen atoms are colored red and blue, respectively. This figure was produced in MOLSCRIPT v2.0 (*30*) and RASTER3D (*21*).

DISCUSSION

Comparison of the Structures of SF1 Peptaibols. The structures of two other members of SF1 have been determined: the crystal structure of alamethicin_F30 (*7*) in MeOH/MeCN and the NMR structure of chrysospermin_C (*8*) bound to dodecylphosphocholine vesicles. All three SF1 structures, alamethicin, trichotoxin, and chrysospermin_C, are amphipathic helices, having two Gln residues, one midway in their sequence and one toward the C-terminus, which form part of the hydrophilic face. Gln6/7 has been shown to be critical for conductance in SF1 members (*34*). Also all have a Pro residue in position 13 or 14 and in the case of alamethicin there is a second Pro residue in position 2. The bend angle seen in chrysospermin_C is ∼38° and in alamethicin it ranges from 10°−30°, as opposed to 8°−10° in the nearly straight trichotoxin. Comparisons of chrysospermin_C and trichotoxin give an average RMSD of 1.59

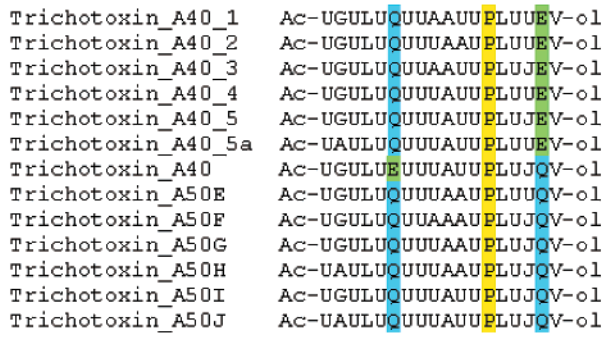

FIGURE 6: The sequences of the two trichotoxin subgroups, the trichotoxin_A40s and the trichotoxin_A50s (*2*−*6*). Pro is in yellow, Glu is in green, and Gln is in blue. U = Aib and J = Iva. Alignments were done in CINEMA (*9*).

Å for their 104 common atoms and ∼1.40 Å for only their backbone atoms. The closest alamethicin structure has an RMSD with trichotoxin of ∼2.37 Å for the 109 common atoms, and ∼1.61 Å for the backbone atoms alone. Thus, there are considerable differences between the SF1 members and this is likely the reason that models based on the alamethicin structure were unsuitable for the molecular replacement of trichotoxin.

Comparison to Structures of Members of Other Peptaibol SFs. The crystal structures of antiamoebin (*12*) from SF2 and Leu[1]-zervamicin (*35*) from SF3 have been determined. The main differences between these two structures and trichotoxin are that zervamicin and antiamoebin have two Hyp and one Pro residue, contributing to a greater bend observed in their structures, thus making zervamicin and antiamoebin significantly shorter. In trichotoxin the Aib carbonyl oxygens contribute to the polar interior; however, in antiamoebin and zervamicin, this is achieved by the carbonyl oxygens of the Hyp residues.

Comparison to Crystal Structures of Trichotoxin Segments. The crystal structures of a number of synthetic trichotoxin segments have been determined, but until now the full peptide had never been crystallized. The structures of trichotoxin segments are considerably different from the comparable regions of the intact molecule. The trichotoxin helix is predominantly α-helix; however, thus far all of the segments examined have been found to be 3_{10}-helix structures. A segment consisting of residues 7−12 (*36*) forms a predominantly right-handed 3_{10}-helix, made up of mostly type III *β*-turns. The N-terminal tripeptide and pentapeptide segments of trichotoxin were both *β*-turns of type I and II, respectively. The first three residues of the pentapeptide were the same in structure as the tripeptide segment (*37*, *38*).

Such differences between segments and the intact peptaibol structure were also seen for alamethicin (*39*). In that case, residues 12−20 were found to contain a mixture of α- and 3_{10}-helix (*40*), whereas an undecapeptide similar to the N-terminus of alamethicin was found to be purely an α-helix (*41*). These results suggest short segments may not necessarily be good models for intact peptaibol molecules.

Structure/Function Relationships of the Trichotoxins. The trichotoxin sequences comprise two subgroups, trichotoxin_A50 and trichotoxin_A40 (Figure 6). The trichotoxin_A50s have two Gln residues, one at position 6, and one at position 17. In the trichotoxin_A40s, one of these Gln residues is replaced by Glu, as found in alamethicin_F30 (*42*). In trichotoxin_A40 the Glu is at position 6, whereas in the other trichotoxins, it is at position 17 (*43*).

Extensive studies have characterized the ability of trichotoxin_A40 and alamethicin_F30 to produce voltage-dependent ion channels in black lipid bilayer membranes (*44*−*47*). Fewer functional studies have been described for the trichotoxin_A50 subgroup, although trichotoxin_A50E has been shown to be capable of forming channels, causing cell death, and capable of lysing most cell and cell organelle membranes (*48*).

Studies involving side chain modifications of the Glu6 residue in trichotoxin_A40 showed that the haemolytic activity was in the order: $(-COO^-) < (-CONHNH_3^+) < (-CONH_2)$, where the modification to an amide makes it equivalent to trichotoxin_A50. Thus, the Gln version is more active in lytic activity than is the version with a Glu residue (*49*). This is comparable to the case for alamethicin where, when the C-terminal Glu is replaced by a Gln, activity increases. Mutational studies have demonstrated that a Glu is not essential for channel-forming activity in the case of alamethicin (*50*). It has been proposed that the Glu residue may cause charge repulsion between monomers in a channel assembly (*49*). Alternatively, it is possible that Glu may have a disruptive effect with regards to channel stability.

Model Channel Features and Implications for the Mechanism of Transport. The trichotoxin_A50E channel was modeled as an octomer (Figure 7), since octamers have been inferred to be the most stable conducting forms of most of the peptaibols. However, conductances have been recorded for a range (4−12) of other peptaibol oligomeric sizes; these result in variable pore sizes, which may produce differences in the mean channel conductances and selectivities for ions (*44*, *51*−*55*). Detailed conductance data is not yet available for trichotoxin, so the number of monomers in this channel is not currently known. However, the octameric model produces a most reasonable channel geometry, as described below, and also, since the alamethicin (*7*) and antiamoebin channels (*56*) have been modeled as octamers, permits direct comparisons to be made between those structures and the trichotoxin channel model produced here.

The Gln6 side chains form a lumen which defines the narrowest region of the pore to have a diameter of ∼2 Å (Figure 8). The Gln6 NE2 atom of one chain can form a hydrogen bond to OE1 of Gln6 of the neighboring helix, a hydrogen bond of ∼3 Å potentially stabilizing the oligomer (Figure 7). This is the residue that forms the interconnecting hydrogen bond with water molecules in the crystal. A second intermolecular hydrogen bond could be formed between the NE2 atom of Gln17 of one helix with the carbonyl oxygen atom of Aib16 of the neighboring helix chain B. Most of the pore lumen is relatively uniform in diameter (∼4−5 Å) as it is composed of nearly straight helices aligned parallel to each other.

Which residues line the pore can be inferred by the hydrogen bonding pattern to solvent in the crystal. Five water molecules form hydrogen bonds to Gly2, Gln6, Ala10, and Gln17 (Table 3). The N atom of Gln17 forms a hydrogen bond with the Pro13 carbonyl oxygen of the same molecule. We suggest that upon application of a voltage, the Gln17 side chains could undergo a change, moving in toward the pore, especially since they have weaker hydrogen bonds of 3.44 Å. This could change the bend angle around Pro13.

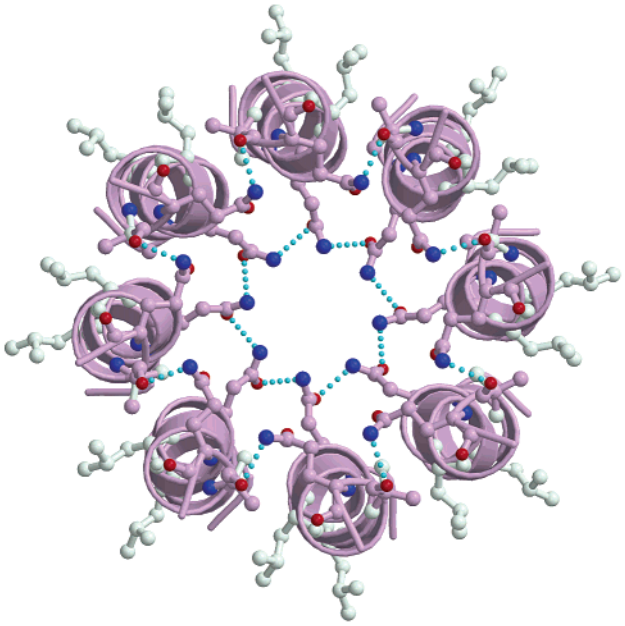

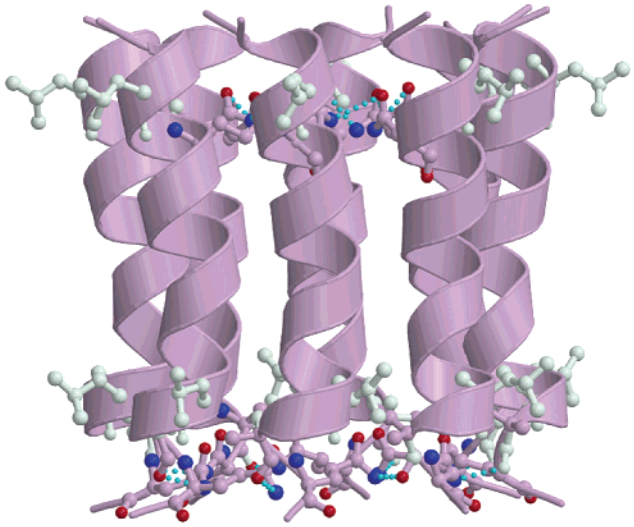

FIGURE 7: (a) A model for an octameric channel of trichotoxin, viewed from the C-terminal end of the helices. The Gln6 and Gln17 residues are depicted in ball-and-stick mode, with their oxygen and nitrogen atoms colored red and blue, respectively. The proposed interhelical hydrogen bonding is shown in cyan. Rings are formed from hydrogen bonds between the Gln6 residues of each helix, and there are additional hydrogen bonds between N of Gln17 and O of Aib16 of neighboring helices. The hydrophobic Leu and Vol residues are shown in ball-and-stick mode in gray on the exterior of the channel. (b) A side view of the channel model. These figures were produced in MOLSCRIPT v.2.0 (*30*) and RASTER3D (*21*).

The voltage could cause the interaction between Pro13 and Gln17 to be broken. The Gln17 side chain could then form a set of interhelical hydrogen bonds similar to those of Gln6. The N-terminus would be part of the intracellular side of the membrane due to inserting first into the membrane. In alamethicin a hinge region similar to trichotoxin is formed by a Gly-Leu-Aib-Pro motif and NMR studies show flexibility in this region (*57*).

The alamethicin channel model comprised of eight monomers, proposed by Fox and Richards (*7*), it is very similar

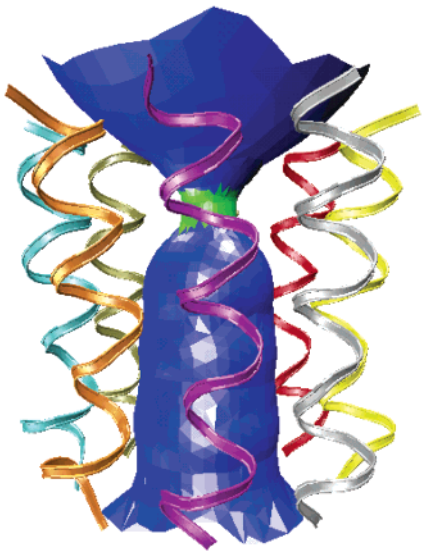

FIGURE 8: Pore dimensions of the octameric channel model. The individual helical monomers are depicted as ribbons in different colors. The blue surface indicates where the pore radius is wide (>2.3 Å), and the green surface indicates where it is <2.3 Å but >1.15 Å. This figure was produced in HOLE (*28*).

to the trichotoxin channel model proposed here, although there are key differences that may result in altered channel-formation and transport capabilities. First, trichotoxin_A50E, lacks the charged Glu residue at the C-terminus which is seen in alamethicin_F30. In addition, alamethicin has a structurally important second Pro residue near the N-terminus and an aromatic Phe residue as its C-terminal residue, both of which are absent in trichotoxin_A50E. The presence of aromatic residues at membrane interfaces has been suggested to stabilize channels in membranes (*58*), so these differences may have functional implications. The Gln6 ring diameter proposed for the alamethicin channel is comparable to that proposed here for trichotoxin. A third possible site of stabilization in alamethicin_F30 was proposed to be the negatively charged Glu near the C-terminus.

Electrostatics calculations on the trichotoxin_A50E channel modeled here suggest the interior of its pore is highly negatively charged. Even without the presence of a Glu residue, this high negative charge suggests that the channel should be selective for cations (Figure 9). Chemical modification studies indicated that the Gln isoform had better lytic activity than the Glu form and thus, may produce far more stable channels (*49*). The electrostatic calculations on the model for trichotoxin_A50E are consistent with replacement by Glu having a disruptive effect on channel stability, as opposed to the stabilization role previously proposed for the equivalent residue in alamethicin.

CONCLUSIONS

Subtle differences in amino acid sequences have been suggested to account for the varying functional activities of SF1 members (*1*). SF1, the largest SF, has the most widely studied range of functions *in vivo*, including such activities as alamethicin causing the release of catecholamines in bovine chromaffin cells (*59*), and chrysospermin_C having some anti-cancer and anti-viral effects (*60*). Other SF1 peptaibols that have not yet been structurally characterized,

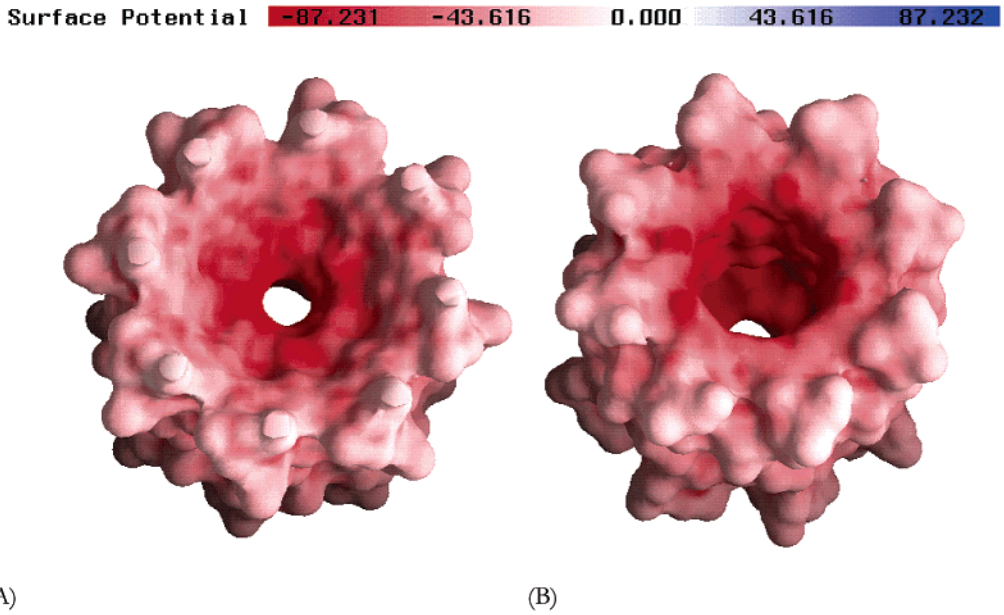

FIGURE 9: Electrostatic surfaces of the octameric channel. (a) viewed from the N-terminus and (b) viewed from the C-terminus. Both ends of the channel have large negative potentials, indicating this should be a cation channel. This figure was produced in GRASP (*26*).

such as the trichosporins, have been described to cause the influx of Ca^{2+} ions into cells (*61*). The trichotoxins are able to form channels and exhibit antibiotic and insecticidal properties (*48*, *49*). Sequence comparisons of the trichotoxins indicates those with a Glu instead of a Gln (trichotoxins A40 vs A50) may be less effective in lytic activity and this can be rationalized from the channel model constructed here. Glu may cause charge repulsion between monomers and thus destabilization of the multimeric channel.

Varying bend angles in the known peptaibol structures due to Pro/Hyp indicate a great deal of flexibility and possible movement in these peptides. It has been shown that prolines in helices are important for their action as hinges (*62*). With lengths sufficient enough to span lipid bilayers, the inferred hydrogen-bonding network indicates how these small single polypeptide helices may associate to form stable larger oligomeric assemblies, producing helical bundle structures, such as the model described in this paper. The Gln residues are conserved in this SF and thus are implicated in the structural hydrogen bonding and in the transport function of the channel. The carbonyl oxygens (in this case from Aib residues) contributing to the polar interior of the channel model, are also seen in gramicidin (*63*) and the KcsA (*64*) channel, and may be common features in many transport systems (*63*). The aromatic residues at the bilayer interface (*58*) in many peptaibols which may act to stabilize the channel, are absent for the trichotoxins. These relatively simple polypeptides form helical bundle structures not unlike the multimeric helical bundle structures found in the KcsA channel.

In summary, these studies have demonstrated the value of peptaibol molecules in channel structure studies. Due to the very high resolution of the crystals, it has been possible to examine more functionally important details and unrestrained structural features than ordinarily possible for larger channel proteins, and the large number of sequence variants in SF1 provide naturally occurring mutants for studying structure−function correlations.

ACKNOWLEDGMENT

We thank Dr. Robert W. Janes for help with crystal mounting, Dr. Simon Teat for help with data collection and processing, and Dr. Ajit Basak and Dr. Nicholas Keep for helpful advice on structure determination and model building. We also thank Dr. Oliver Smart for running HOLE on the model structure.

REFERENCES

1. Chugh, J. K., and Wallace, B. A. (2001) *Biochem. Soc. Trans. 29*, 565−570.
2. Brückner, H., König, W. A., Greiner, M., and Jung, G. (1979) *Angew. Chem., Int. Ed. Engl. 18*, 476−477.
3. Jaworski, A., and Brückner, H. (1999) *J. Chromatogr. 862*, 179−189.
4. Przybylski, M., Dietrich, I., Manz, I., and Brückner, H. (1984) *Biomed. Mass Spectrosc. 11*, 569−582.
5. Brückner, H., and Przybylski, M. (1984) *J. Chromatogr. 296*, 263−275.
6. Brückner, H. (1986) in *Peptides, Proceedings of the 19th European Peptide Symposium* (Theodoropoulos, D., Ed.) pp 231−234, de Gruyter, Berlin.
7. Fox, R. O., Jr., and Richards, F. M. (1982) *Nature 25*, 325−330.
8. Anders, R., Ohlenschlager, O., Soskic, V., Wenschuh, H., Heise, B., and Brown, L. R. (2000) *Eur. J. Biochem. 267*, 1784−1794.
9. Parry-Smith, D. J., Payne, A. W. R., Michie, A. D., and Attwood, T. K. (1998) *Gene 211*, GC45-GC46.
10. SHELXTL (1997) Bruker AXS, Inc., Madison, WI 53719-1173.
11. Matthews, B. W. (1968) *J. Mol. Biol. 33*, 491−497.
12. Snook, C. F., Woolley, G. A., Pattabhi, V., Wood, S. P., Blundell, T. L., and Wallace, B. A. (1998) *Structure 6*, 783−792.
13. Navaza, J. (1994) *Acta Crystallogr., Sect. A 50*, 157−163.
14. Vagin, A., and Teplyakow, A. (1997) *J. Appl. Crystallogr. 30*, 1022−1025.
15. SYBYL 6.7. Tripos Inc., 1699 South Hanley Rd., St. Louis, MO 63144.
16. Sheldrick, G. M., and Schneider, T. R. (1997) *Methods Enzymol. 277*, 319−343.
17. Lamzin, V. S., and Wilson, K. S. (1993) *Acta Crystallogr., Sect. D 49*, 129−147.
18. Jones, T. A., Zou, J. Y., Cowan, S. W., and Kjeldgaard, M. J. (1991) *Acta Crystallogr., Sect A 47*, 110−119.
19. Kleywegt, G. J., and Jones, T. A. (1998) *Acta Crystallogr., Sect. D 54*, 1119−1131.

20. Esnouf, R. (1997) *J. Mol. Graph. 15*, 133−138.
21. Merrit, E. A., and Bacon, D. J. (1997) *Methods Enzymol. 277*, 505−524.
22. Laskowski, R. A., MacArthur, M. W., Moss, D. S., and Thornton, J. M. (1993) *J. Appl. Crystallogr. 26*, 283−291.
23. Hutchinson, E. G., and Thornton, J. M. (1994) *Protein Sci. 3*, 2207−2216.
24. Hutchinson, E. G., and Thornton, J. M. (1996) *Protein Sci. 5*, 212−220.
25. Driessen, H., Haneef, M. I. J., Harris, G. W., Howlin, B., Khan, G., and Moss, D. S. (1989) *J. Appl. Crystallogr. 22*, 510−516.
26. Nicholls, A., Sharp, K., and Honig, B. (1991) *Proteins: Struct., Funct., Genet. 11*, 281−296.
27. Weiner, S. J., Kollman, P. A., Nguyen, D. T., and Case, D. A. (1986) *J. Comput. Chem. 7*, 230.
28. Smart, O. S., Goodfellow, J. M., and Wallace, B. A. (1993) *Biophys. J.* 65, 2455−2460.
29. Collaborative Computational Project: Number 4. (1994) *Acta Crystallogr., Sect. D 50*, 760−763.
30. Kraulis, P. J. (1991) *J. Appl. Crystallogr. 24*, 946−950.
31. Rizzo, V., Schwarz, G., Voges, K. P., and Jung, G. (1985) *Eur. Biophys. J. 12*, 67−73.
32. Sevcik, J., Dauter, Z., Lamzin, V. S., and Wilson, K. S. (1996) *Acta Crystallogr., Sect. D 50*, 327−344.
33. Teeter, M. M., Roe, S. M., and Heo, N. H. (1993) *J. Mol. Biol. 230*, 292−311.
34. Kaduk, C., Dathe, M., and Bienert, M. (1998) *Biochim. Biophys. Acta 1373*, 137−146.
35. Karle, I. L., Flippen-Anderson, J. L., Agarwalla, S., and Balaram, P. (1991) *Proc. Natl. Acad. Sci. U.S.A. 88*, 5307−5311.
36. Kokkinidis, M., Tsernoglou, D., and Brückner, H. (1986) *Biochem. Biophys. Res. Commun. 136*, 870−875.
37. Gessmann, R., Brückner, H., and Kokkinidis, M. (1991) *Pept. Res. 4*, 239−244.
38. Gessmann, R., Brückner, H., and Kokkinidis, M. (1991) *Biochem. Biophys. Res. Commun. 174*, 878−884.
39. Bosch, R., Jung, G., Schmitt, H., Sheldrick, G. M., and Winter, W. (1984) *Angew. Chem., Int. Ed. Engl. 26*, 450−453.
40. Bosch, R., Jung, G., Schmitt, H., and Winter, W. (1985) *Biopolymers 24*, 961−978.
41. Bosch, R., Jung, G., Schmitt, H., and Winter, W. (1985) *Biopolymers 24*, 979−999.
42. Brückner, H., Bokel, M., and Przybylski, M. (1985) in *Peptides, Structure and Function, Proceedings of 9th American Peptide Symposium* (Deber, C. M., Hruby, V. J., and Kopple, K. D., Eds.) pp 108−112, Pierce Chemical Co., Rockford, IL.
43. Brückner, H., and Jung, G. (1979) in *Peptides, Structure and Biological Function, Proceedings of 6th American Peptide Symposium* (Gross, E., and Meienhofer, J., Eds.) pp 723−726, Pierce Chemical Co., Rockford, IL.
44. Boheim, G. (1974) *J. Membr. Biol. 19*, 277−303.
45. Boheim, G., Irmscher, G., and Jung, G. (1978) *Biochim. Biophys. Acta 507*, 485−506.
46. Mueller, P., and Rudin, D. O. (1968) *Nature 217*, 713−719.
47. Hanke, W., Methfessel, C., Wilmsen, H. V., Katz, E., Jung, G., and Boheim, G. (1982) *Biochim. Biophys. Acta 507*, 108−114.
48. Matha, V., Jegorov, A., Kiess, M. T., and Brückner, H. (1992) *Tissue Cell 24*, 559−564.
49. Jung, G., Brückner, H., Oekonomopulos, R., Boheim, G., Breitmaier, E., and König, W. A. (1979) in *Peptides, Structure and Biological Function, Proceedings of the 6th American Peptide Symposium* (Gross, E., and Meienhofer, J., Eds.) pp 647−654, Pierce Chemical Co., Rockford, IL.
50. Molle, G., Duclohier, H., Julien, S., and Spach, G. (1991) *Biochim. Biophys. Acta 1064*, 365−369.
51. Sansom, M. S. P. (1993) *Q. Rev. Biophys. 26*, 365−421.
52. Sansom, M. S. P. (1993) *Eur. Biophys. J. 22*, 105−124.
53. Breed, J., Biggins, P. C., Kerr, I. D., Smart, O. S., and Sansom, M. S. P. (1997) *Biochim. Biophys. Acta 1325*, 235−249.
54. Baumann, G., and Mueller, P. (1974) *J. Supramol. Struct. 2*, 538−557.
55. Duclohier, H., Snook, C. F., and Wallace, B. A. (1998) *Biochim. Biophys. Acta 1415*, 255−260.
56. Wallace, B. A., Snook, C. F., Duclohier, H., and O'Reilly, A. O. (2000) in *Peptides for the New Millenium: Proceedings of the 16th of the American Peptide Symposium* (Fields, G. B., Tam, J. P., & Barany, G., Eds.) pp 733−335, Kluwer Academic Publishers, Dordrecht.
57. Gibbs, N., Sessions, R. B., Williams, P. B., and Dempsey, C. E. (1997) *Biophys. J. 72*, 2490−2495.
58. Wallace, B. A., and Janes, R. W. (1999) *Adv. Exp. Med. Biol. 467*, 789−99.
59. Dathe, M., Kaduk, C., Tachikawa, E., Melzig, M. F., Wenschuh, H., and Bienert, M. (1998) *Biochim. Biophys. Acta 1370*, 175−183.
60. Kim, Y. H., Yeo, W. H., Kim, Y. S., Chae, S. Y., and Kim, K. S. (2000) *J. Microbiol. Biotech. 10*, 522−528.
61. Tachikawa, E., Nogimori, K., Takahashi, S., Mizuma, K., Itoh, K., Kashimoto, T., Nagaoka, Y., Iida, A., and Fujita, T. (1996) *Biochim. Biophys. Acta 1282*, 140−148.
62. Sansom, M. S. P., and Weinstein, H. (2000) *Trends Pharmacol. Sci. 21*, 445−451.
63. Wallace, B. A. (2000) *Bioessays 22*, 227−234.
64. Doyle, D. A., Cabral, J. M., Pfuetzner, R. A., Kuo, A. L., Gulbis, J. M., Cohen, S. L., Chait, B. T., and MacKinnon, R. (1998) *Science 280*, 69−77.

BI026150Z